


RESEARCH

Open Access



# Modelling and analysis of three-phase grid-tied photovoltaic systems

Abraham Dandoussou<sup>1,2,3\*</sup>  and Pierre Kenfack<sup>1</sup>

\*Correspondence:  
abraham.dandoussou@ubuea.  
cm

<sup>1</sup> Department of Electrical  
and Power Engineering, Higher  
Technical Teachers' Training  
College (HTTTC), Kumba,  
University of Buea, Kumba,  
Cameroon

<sup>2</sup> Laboratoire d'Energie, Signal,  
Imagerie et Automatique  
(LESIA), National School  
of Agro-Industrial Sciences,  
University of Ngaoundere,  
Ngaoundere, Cameroon

<sup>3</sup> Department of Science  
and Engineering Techniques,  
School of Chemical Engineering  
and Mineral Industries, University  
of Ngaoundere, Ngaoundere,  
Cameroon

## Abstract

The global warming of the planet is as a result of human activities. Fossil fuel depletion and its high prices have caused a worldwide economic instability; governments around the world turn to alternative energy sources that are pollution-free. Solar photovoltaic system is one of the biggest renewable energy resources to generate electrical power and the fastest growing power generation in the world. The objectives of this work are: to ensure the maximum power point tracking (MPPT) in the side of the PV panels, to ensure the DC–DC boost converter boosts DC voltage by using the MPPT algorithm and pulse width modulation (PWM) technique, to invert the boosted DC voltage to three-phase AC voltages by using sine PWM technique to five-level VSI, to synchronize the PV-generated power to the grid power aided by the synchronous reference frame (SRF) controller. The step of modelling the photovoltaic system with MATLAB/Simulink was performed with RL-load and L-load and %THD got through FFT analysis. The results show that the DC voltage generated by the PVA produces an AC current sinusoidal at the output of the inverter. The contribution of the PV system to the grid consequently reduces the power fluctuation of the grid.

**Keywords:** MPPT algorithm, DC–DC boost converter, Five-level VSI, Synchronous reference frame (SRF), MATLAB/Simulink

## Introduction

Power demand has increased drastically in societies due to the growing population and industries to meet up with the innovation of ever rising inventions. The power outage rate is high; thus, it can be reduced by connecting additional power generator to support the existing one. This leads to an alternate power generator (solar power) to support the already existing power generator by connecting the solar system tied to an analysed interface of a three-phase utility grid.

Focusing on renewable energy sources (solar plants, hydropower plants, wind farms, biogas plants, and tidal wave units) is impeding on daily due to the failures conferred by the conventional fossil fuel power generation (diesel generators, thermal plants, and nuclear plants); the massive exhaustion and the tremendous environmental hazards they produce [1]. Hydropower is a big power-generating plant and can be used for a massive load demand among the listed renewable sources, but its build-up takes years and its installation is expensive. As a result, wind farms are looked at for replacement, which

also generate huge power but in areas far from where the power can be used. Hence, it can be concluded that solar plants are the best power generator in either small or large quantities [2–7].

Solar irradiation from the sun when carefully harnessed can generate direct current (DC) power through a set of photovoltaic arrays (PVA). As the single-phase AC or the three-phase AC loads run on AC voltage, the DC power generated from the PVA should be converted to either of single-phase AC or three-phase AC. Studies and researches are ongoing on the modes of conversion with respect to various converters in order to improve the efficiency and to reduce harmonic generation. It has been seen by many authors on how the idea of multilevel converters can be used; these converters were introduced in 1975 [8]. It has been proposed that the three major topologies for three-phase grid-tied multilevel converters for PV systems are: the cascaded H-bridge, the diode-clamped and the flying capacitor multilevel converters [9–15]; all are complicated circuits and control problems. Previous researchers used conventional voltage source inverter (VSI) for transforming DC voltage received from the PVA to AC voltage for injection to the utility grid. This six-switch two-level VSI requires large inductor capacitor (LC) filters for high harmonics reduction, produced by the inverter; thus, high installation cost of the PV plant for transmission of large power is required. The unit vector template feedback control is used, which takes inputs only from the grid. As the result, this converter and the controller are replaced by a five-level VSI and a synchronous reference frame (SRF) controller that gets feedback from the grid voltages, currents, and DC voltages of the inverter. Also, the materials that are used as well as the methods that are applied to model the PV system are described in the section below.

## Materials and methods

### Modelling of the photovoltaic array

This is a DC source that converts solar irradiance incident on it to generate power. Each panel on the array is made up of  $p$ -type and  $n$ -type materials with silicon doping to produce holes and electrons, respectively. The input variables to the PV array are: irradiance and ambient temperature, whereas the output is a voltage signal. With changes in weather conditions, the DC voltage from the PVA varies and cannot be used as input to the five-level VSI. Thus, the PVA is connected to a stabilizing DC-regulated booster converter, which can maintain the output voltages at a particular value for constant DC voltage generation. The single IGBT<sub>b</sub> switch of the boost converter compares duty ratios generated by the incremental conductance MPPT algorithm. The increase or decrease in duty ratio value is gotten from the ratio comparison errors of voltage and current of the PVA. Without loss of generality, a rise in solar irradiation causes a decrease in duty ratio, while a drop in solar irradiation causes an increase in duty ratio [2]. The boost converter achieves MPP through the incremental conductance MPPT algorithm. A PV cell is represented in Fig. 1 by an electrical equivalent of one diode, series resistance  $R_s$  and parallel resistance  $R_p$ . The various parameters that characterize the PV cell above, in the equations below, can be found in [17] and the manufacturer of the solar module; Sun Power (SPR-305)—WT also gives the other parameters required to model the solar cells. The datasheet gives the electrical characteristics calculated under the standard test condition (STC) when the temperature  $T$  is 25 °C and the irradiance  $G$  is 1000 W/m<sup>2</sup>.

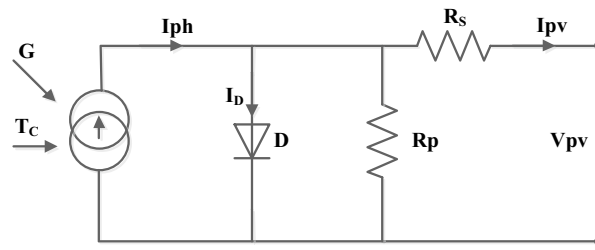


**Fig. 1** Model of a PV cell

**Table 1** Data specifications for the Solar Module SPR-305-WHT-U

Parameters	Symbol	Value
Maximum power	Pm	305.226 W
Short-circuit current	Isc	5.96 A
Open-circuit voltage	Voc	64.2 V
Maximum power point voltage	Vmp	54.7 V
Maximum power point current	Imp	5.58 A
Number of cells per module	Ncell	96
Light-generated current	Iph	6.0004 A
Diode saturation current	I <sub>0</sub>	6.3004e-12
Diode ideality factor	a	0.94497
Shunt resistance	Rp	292.7209 Ω
Series resistance	Rs	0.3721 Ω
Power needed	Pneed	10 kW
Total number of PV modules	N	5 × 7 = 35

The solar cell is modelled and then extended to the model of a PV module and finally the model of a PV array. The output current of the PV cell is:

$$I_{pv} = I_{ph} - I_0 \left[ \exp \left( \frac{(qV + R_s I_{pv})}{akT} \right) - 1 \right] - \frac{V_{pv} + R_s I_{pv}}{R_p} \tag{1}$$

The current–voltage (*I–V*) characteristics curve of a PV array made up of 35 PV panels (SunPower SPR-305-WHT-U with specifications shown in Table 1) as shown in Fig. 2 is nonlinear and crucially depends on the temperature and the solar irradiation. As represented in Fig. 2, when the irradiation increases, the current increases more than the voltage and thus the power also increases. And when the temperature increases, the current decreases and thus the power decreases too. The PV system has to operate at the MPP, which is made possible through an INC MPPT algorithm.

**Modelling of the boost converter and the incremental conductance MPPT technique**

The DC–DC boost converter is used to increase of the input voltage of a five-level VSI from the PVA since AC loads work on high voltages. This boost converter is made up of a single IGBT<sub>b</sub>/diode switch, capacitor (*C<sub>b</sub>*), inductor (*L<sub>b</sub>*) and diode. It is the main tool for obtaining the MPP. The voltage ratio for a boost converter is gotten from the time integral of the inductor voltage by equating it to zero over a switching period. The voltage ratio is

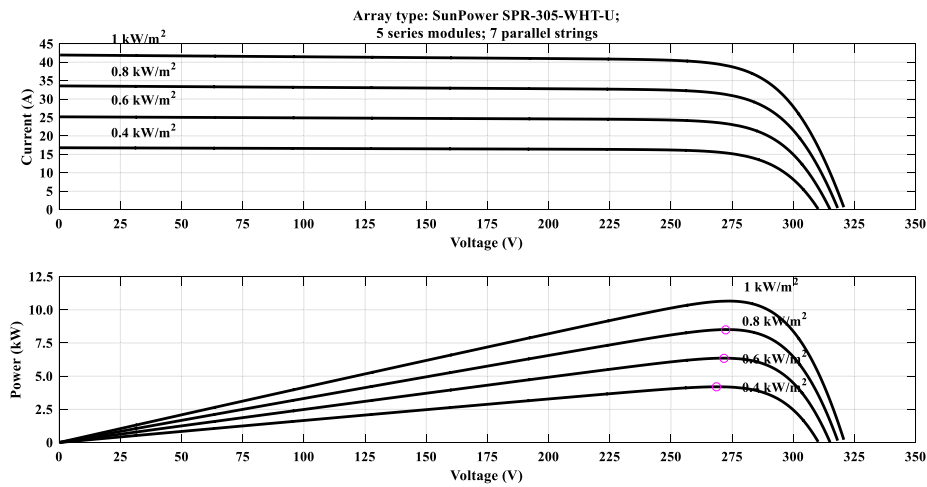


**Fig. 2** Characteristics of PV at constant temperature of 25 °C

equivalent to the ratio of the switching period to the off time of the switch  $T$  ( $IGBT_b$ ) such that:

$$\frac{V_{out}}{V_{in}} = \frac{T}{t_{off}} = \frac{1}{1 - D} \tag{2}$$

From Eq. (2), the duty ratio  $D$  is given as:

$$D = 1 - \frac{V_{in}}{V_{out}} \tag{3}$$

The incremental conductance algorithm, as shown in Fig. 3, is based on the fact that the slope of the PV array power curve is zero at the MPP, positive on the left of the MPP, and negative on the right of the MPP, as given by the equations below:

$$\frac{dP}{dV} = 0, \quad \text{at MPP} \tag{4}$$

$$\frac{dP}{dV} > 0, \quad \text{left of MPP} \tag{5}$$

$$\frac{dP}{dV} < 0, \quad \text{right of MPP} \tag{6}$$

Since  $\frac{dP}{dV} = I + V \frac{dI}{dV} \cong I + V \frac{\Delta I}{\Delta V}$ , Eqs. (4), (5) and (6) give the tracking point (incremental conductance), respectively, as:

$$\frac{\Delta I}{\Delta V} = -\frac{I}{V}, \quad \text{at MPP} \tag{7}$$

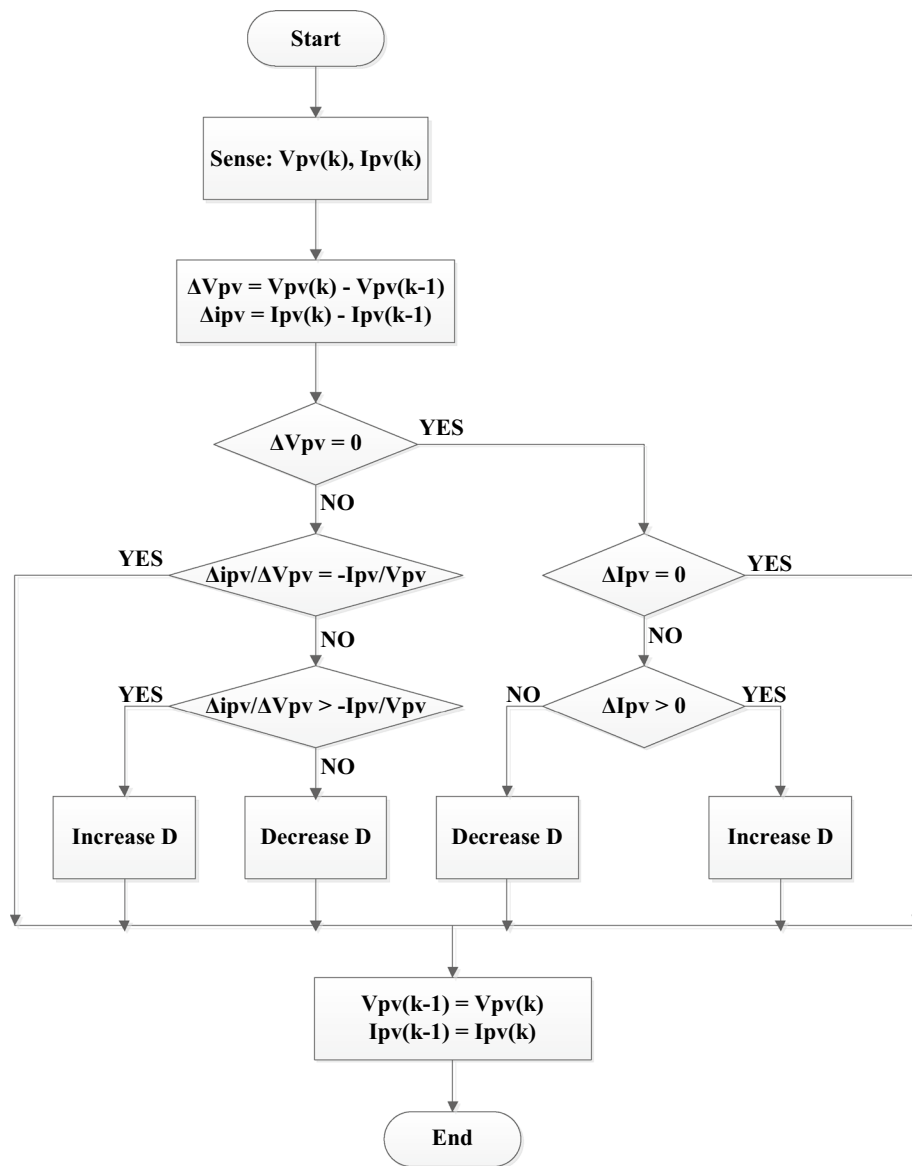


**Fig. 3** Flowchart for MPPT by incremental conductance algorithm

$$\frac{\Delta I}{\Delta V} > -\frac{I}{V}, \quad \text{left of MPP} \tag{8}$$

$$\frac{\Delta I}{\Delta V} < -\frac{I}{V}, \quad \text{right of MPP} \tag{9}$$

**Modelling of the five-level voltage source inverter**

A five-level VSI, as shown in Fig. 4, has interconnected capacitors to stabilize and to overshoot the ripple of the output voltages. Since its output voltages have five levels:  $V_{DC}$ ,  $V_{DC}/2$ ,  $0$ ,  $-V_{DC}/2$  and  $-V_{DC}$ , it is called a five-level inverter. The input voltage is from the PVA through the DC–DC boost converter which DC voltage with half

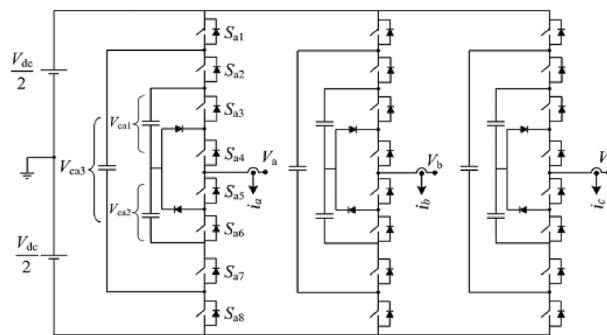


**Fig. 4** A five-level voltage source inverter circuit

the voltage  $V_{DC}/2$  connected through a common neutral point. Also, it is made up of splitting capacitors that generate different voltage levels for switching on/off eight switches (IGBT/diode) on each of the three legs, and diodes for clamping. The diode-clamped and the flying-capacitor inverter topologies are used for the realization of this topology as seen in Fig. 4 with the number of clamping diodes lower than the number in the diode-clamped inverter, and the number of capacitors is also lower than that in the flying capacitor inverter. This inverter is expected to transform the DC power from the PVA to a three-phase AC power fed to the utility grid controlled by a SFR controller module that will produce reference signals to enable the converter to work in synchronization with the utility grid. The capacitors C1, C2, and C3 are for voltage splitting, thus generating various voltage levels for switching. The DC source used need not to be isolated at the input for regenerative applications. The capacitors  $C_{x1}$  and  $C_{x2}$  with  $x = a, b, c$  are charged. The five-level voltages are generated as per the switching of the eight switches of one leg with the zero-voltage level in charge of discharging and charging the capacitors for achieving voltage across capacitor equalizing, making the converter redundant to voltage variations. The switching states are achieved by sinusoidal PWM technique with reference sine waveform compared to four-level-shifted high-frequency triangular waveforms.

In phase disposition (PD), the carrier modulation technique is the method used for pulse generation where all the carrier waveforms are in phase with no phase shift. The reference sine waveform for the above PD modulation technique is generated by the SRF controller, which generates a reference signal in synchronization to the grid [2].

There exists a redundancy of switching states at levels 1, 2, 3 to charge and to discharge capacitors and no redundancy of switching states at levels 0 and 4. At level 1 capacitor voltages  $V_{C_{x3}}$  and  $V_{C_{x2}}$  are managed, and at level 3 capacitor voltages  $V_{C_{x3}}$  and  $V_{C_{x1}}$  are controlled. Each redundancy state has three capacitors to charge and to discharge with respect to the output current direction, thus decreasing the difference between nominal and measured voltage levels. Furthermore, if the currents flowing through the capacitors to discharge and to charge capacitors C1, C2, and C3 are not regulated, the flying capacitors voltage may differ from what was expected.

The switching sequence for the switches on the first leg (Phase A) is the same switching sequence for both Phases B (Sa9–Sa16) and C (Sa17–Sa24), where the first four switches on each leg stand for the positive section of that leg and the remaining

four switches for the negative section for Phase A. In order to achieve this complementary setting, a NOT gate is used as a logical operator.

Equation (10) gives the possible change in voltages for the given capacitor as:

$$\Delta V_{cxi} = V_{cxi} - V_{cxi,ref} \tag{10}$$

where  $i = 1, 2$  and  $3$  and  $x = a, b$  and  $c$ ,  $V_{cxi}$  are capacitor voltages,  $V_{cxi,ref}$  are the monetary values

$$V_{cxi,ref} = \frac{iV_{dc}}{4}, \text{ for } i = 1, 2, 3.$$

$V_{cxi}$  should be set close to zero to accomplish capacitor voltage balancing.

**Modelling of the synchronous reference frame controller**

This is a module brought up in [2, 16] to test the control of the multilevel inverter’s output voltage in order to match to the grid voltage amplitude, phase and frequency, by taking feedback from the grid three-phase voltages, currents and DC link voltage at the input (as shown in Fig. 5). It should be noted that the DC link in the feedback loop is obtained after currents are converted to  $d$ -axis and  $q$ -axis.

Park’s transformation is used by the SRF controller for controlling the current of the inverter with the  $dq$  components of the currents calculated for the phase-locked loop (PLL) module working in synchronization to the grid voltage. Let  $r$  be a vector in the  $abc$  coordinate system with the angle between  $a$  and  $b$ ,  $b$  and  $c$ , and  $c$  and  $a$  being 120 degrees. Then, from [16] Eq. (11) is defined:

$$\vec{r} = r_a \cdot \hat{a} + r_b \cdot \hat{b} + r_c \cdot \hat{c} \tag{11}$$

where  $r_x$ , (for  $x = a, b, c$ ) are projections of the vector  $r$  in the directions  $a, b$  and  $c$ , respectively.

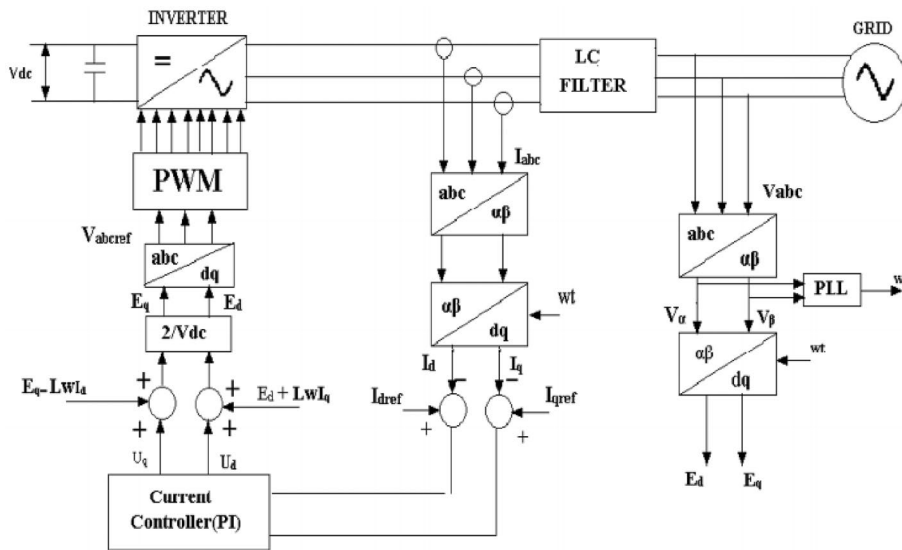


**Fig. 5** SRF control structure for PVA grid interconnection

Also, in the  $\alpha\beta$  coordinate system we have the vector  $r$  given as:

$$\vec{r} = r_\alpha \cdot \hat{\alpha} + r_\beta \cdot \hat{\beta} \tag{12}$$

where  $r_\alpha$  and  $r_\beta$  are projections of the  $r$  vector in direction of  $\alpha$  and  $\beta$ , respectively. The relation between  $\alpha\beta$  and  $abc$  is gotten as demonstrated below:

Firstly, the projection of vector  $r$  in the  $\alpha$ -direction,  $r_\alpha$  is given by

$$\begin{aligned} r_\alpha &= \vec{r} \cdot \hat{\alpha} \\ r_\alpha &= r_a - \frac{1}{2}r_b - \frac{1}{2}r_c \end{aligned} \tag{13}$$

Also,  $r_\beta$  projection of  $r$  vector in the direction of  $\beta$  is given by:

$$\begin{aligned} r_\beta &= \vec{r} \cdot \hat{\beta} \\ r_\beta &= \frac{\sqrt{3}}{2}r_b - \frac{\sqrt{3}}{2}r_c \end{aligned} \tag{14}$$

Thus,

$$\begin{pmatrix} r_\alpha \\ r_\beta \\ 0 \end{pmatrix} = \begin{pmatrix} 1 & -\frac{1}{2} & -\frac{1}{2} \\ 0 & \frac{\sqrt{3}}{2} & -\frac{\sqrt{3}}{2} \\ \frac{1}{\sqrt{2}} & \frac{1}{\sqrt{2}} & \frac{1}{\sqrt{2}} \end{pmatrix} \begin{pmatrix} r_a \\ r_b \\ r_c \end{pmatrix} \tag{15}$$

And,

$$\begin{pmatrix} r_d \\ r_q \\ 0 \end{pmatrix} = \begin{pmatrix} \cos \theta & \sin \theta & 0 \\ -\sin \theta & \cos \theta & 0 \\ 0 & 0 & 1 \end{pmatrix} \begin{pmatrix} 1 & -\frac{1}{2} & -\frac{1}{2} \\ 0 & \frac{\sqrt{3}}{2} & -\frac{\sqrt{3}}{2} \\ \frac{1}{\sqrt{2}} & \frac{1}{\sqrt{2}} & \frac{1}{\sqrt{2}} \end{pmatrix} \begin{pmatrix} r_a \\ r_b \\ r_c \end{pmatrix} \tag{16}$$

By using Clark's transformation and from  $\alpha\beta$ -coordinates to  $dq$ -coordinates (Parks transformation), Eq. (17) is obtained.

$$\begin{pmatrix} r_d \\ r_q \\ 0 \end{pmatrix} = \sqrt{\frac{2}{3}} \begin{pmatrix} \cos \theta & -\frac{1}{2} \cos \theta + \frac{\sqrt{3}}{2} \sin \theta & -\frac{1}{2} \cos \theta - \frac{\sqrt{3}}{2} \sin \theta \\ -\sin \theta & \frac{1}{2} \sin \theta + \frac{\sqrt{3}}{2} \cos \theta & \frac{1}{2} \sin \theta - \frac{\sqrt{3}}{2} \cos \theta \\ \frac{1}{\sqrt{2}} & \frac{1}{\sqrt{2}} & \frac{1}{\sqrt{2}} \end{pmatrix} \tag{17}$$

The  $dq$  axis calculation for the given controller is given in the equations below [2]:

$$[U_\alpha U_\beta]^T = \left(\frac{2}{3}\right) \left[1 - 1/2 - 1/2; 0\sqrt{3}/2 - \sqrt{3}/2\right]^T [U_a U_b U_c]^T \tag{18}$$

$$[U_d U_q]^T = [U_\alpha U_\beta]^T [\cos \omega t \sin \omega t - \sin \omega t \cos \omega t] \tag{19}$$



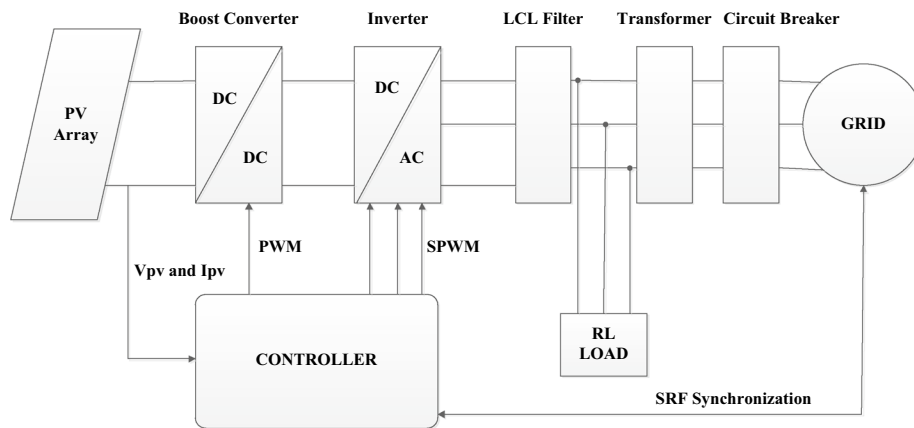


**Fig. 6** Basic block diagram of the grid-tied PV system

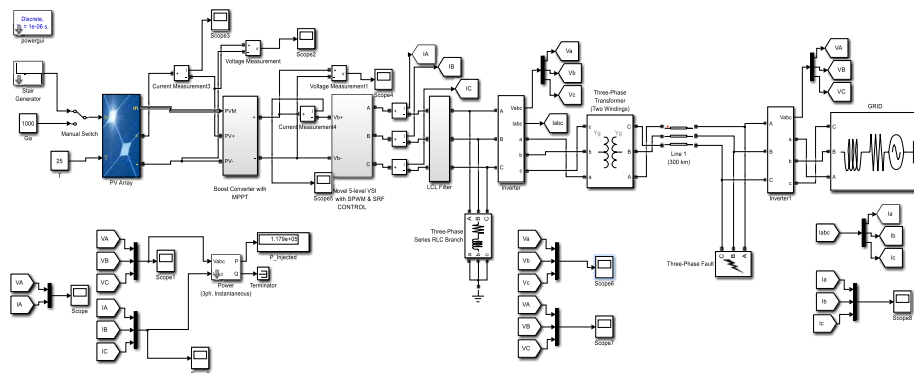


**Fig. 7** Simulink model of the whole PV grid-tied system

The function  $U$  denotes either three-phase voltages or currents. The voltage controller is a PI controller with input taken by comparison between the DC voltage at the DC link capacitor and the reference value given by the user. The output of the voltage controller is direct axis component reference and the quadrature axis reference component is considered to be 0. The current controller produces the needed reference  $dq$  voltage reference component with the PI controllers in it. The reference  $dq$  voltage components ( $U_d^*$  and  $U_q^*$ ) are converted to sinusoidal by reverse Park's transformation [16]. The final three-phase sinusoidal reference waveforms are compared to the phase disposition multicarrier modulation technique for the generation of pulses for the five-level inverter. As the SRF controller uses PLL to generate the reference signals and the PLL is operated with grid voltage as feedback, the inverter operates in synchronization with the grid.

It should be noted that the current PI controllers are used to control the grid current, through the DC link voltage. Their inputs are obtained from currents  $I_d$  and  $I_q$ , and their outputs are the reference voltages  $U_d$  and  $U_q$ . Parameters  $k_p$  and  $k_i$  of these PI controllers are tuned using trial-and-error method.

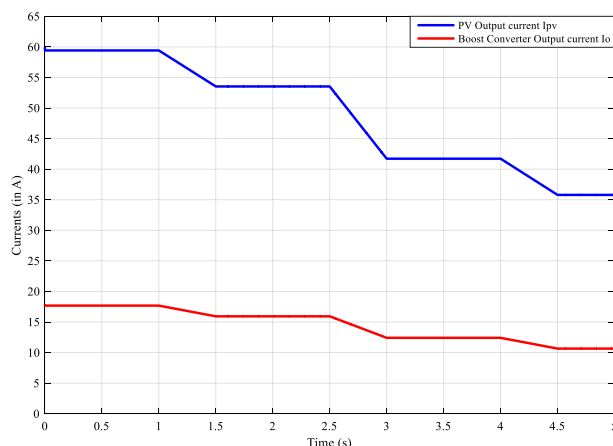


**Fig. 8** Current generated by the PVA versus boosted current from the PVA by boost converter

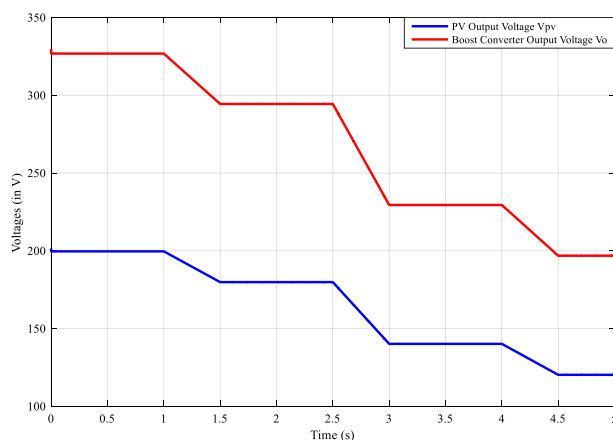


**Fig. 9** Voltage generated by the PVA versus boosted voltage from the PVA by boost converter

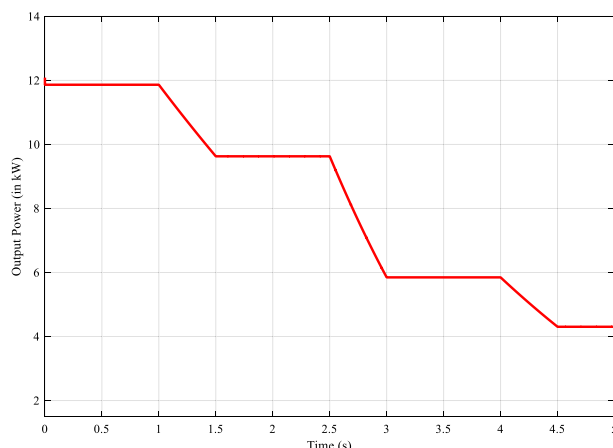
**Modelling of the grid-tied PV system**

Figure 6 shows the block diagram of the grid-tied PV system. Using MATLAB/SIMULINK, the whole system has been modelled as shown in Fig. 7. The grid is a 10-kV which has been stepped down to 400 V. The temperature at the surface of the PV array has been taken as constant and equal to 25 °C, while the irradiance varies as follows: 1000–900–700–600 W/m<sup>2</sup>. The RL load has  $R = 53 \Omega$  and  $L = 529 \text{ mH}$ . Simulations are done under normal operation (no faults or shadow) and also under faulty conditions (shadow, grid phase failure, etc.).

**Results and discussion**

**Validation of the MPPT algorithm**

Figures 8, 9, and 10 show the currents, the voltages, and the powers at the output of the PV array and at the output of the boost DC–DC converter. It should be noted that the boost converter is controlled by an incremental conductance MPPT algorithm. From the obtained results, it is clear that there is an increase in power transferred to the grid. With the fluctuation of the weather conditions, especially the irradiance which changes



**Fig. 10** Power generated by the PVA versus boosted power from the PVA by boost converter

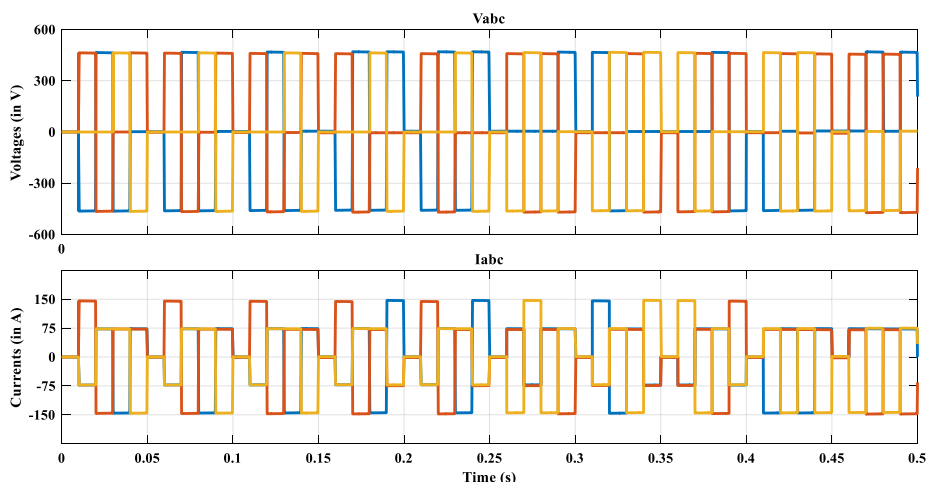


**Fig. 11** Output voltages from the five-level VSI without a pure sine circuit

from 1000 to 600 W/m<sup>2</sup>, the transferred power drops from 12 to 4 kW, which is still sufficient for the load to operate properly.

**Validation the three-phase inverter**

Figure 11 shows the output voltages of the three-phase PV inverter used in this work. The results show that thus the voltages are periodic, they are not sinusoidal. In other to obtain sinusoidal voltages, a pure sine circuit generator made up of LC filters has been added to the output of the inverter. The results are shown in Fig. 12 where the output voltages are now sinusoidal, with respect to the grid voltages. These voltages can now be synchronized with the grid one, in order to allow the load to operate properly (without disturbances). The obtained results are clearly better than those obtained in previous researches like in [6, 13, 15, 16].

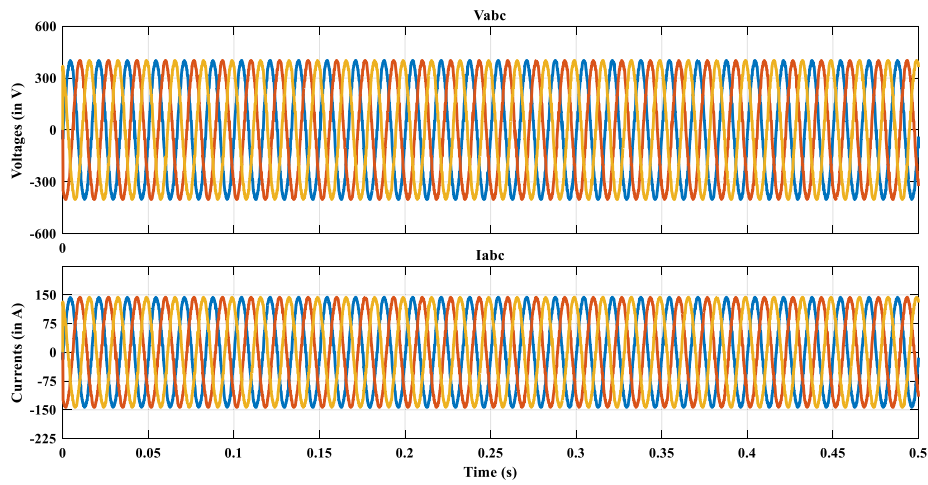


**Fig. 12** Output voltages from the five-level VSI with a pure sine circuit

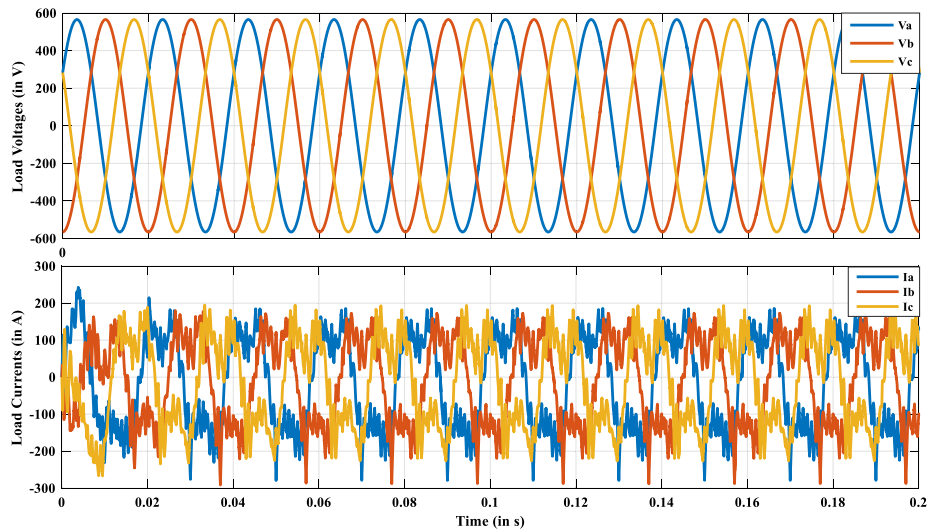


**Fig. 13** Load voltage and current for three-phase RL-load

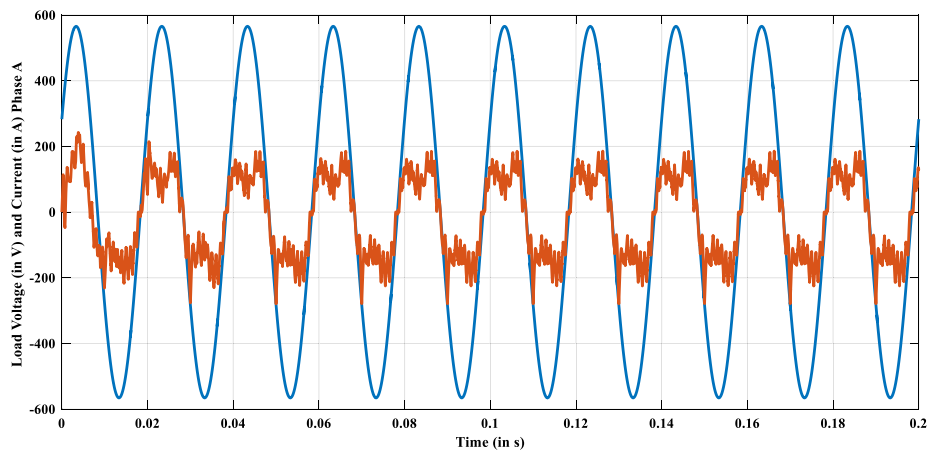


**Fig. 14** Va and Ia phase check of the RL-load

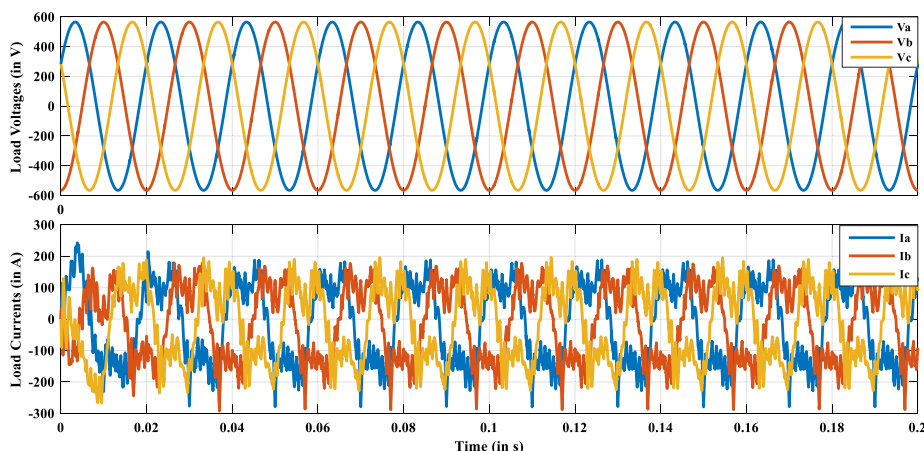


**Fig. 15** Load voltage and current for three-phase inductive load

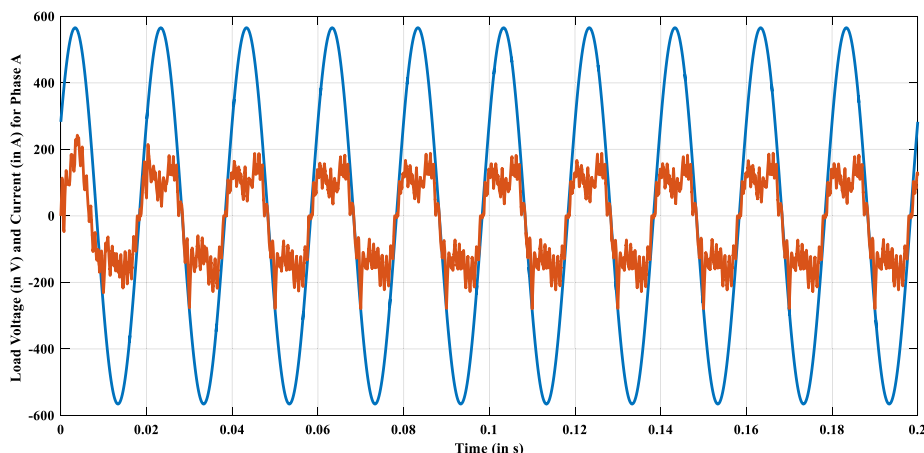


**Fig. 16**  $V_a$  and  $I_a$  phase check of the L-load

**Load voltages and currents**

The simulations have done with  $R-L$  load and with an inductive ( $L$ ) load. The voltages and the currents at the terminals of the load are represented in Figs. 13 and 14, for an  $R-L$  load, and in Figs. 15 and 16 for an inductive load. These results are obtained under normal operating conditions (no failure from the grid or from the PV array side). In this case, voltage and current waveforms are normal, with the total harmonics distortion (THD), which is practically equal to zero (see Figs. 17, 18). In order to check the robustness of the control strategy of this system, simulations have also been done with failure in one or another. In Fig. 19, grid Phase B failure has been introduced at  $t=0.25$  s as seen in Fig. 19a. It can be observed that before and after this time, the load voltages and currents have not changed. This means that the PV array continues to supply the load properly Fig. 19b. In Fig. 20, the failure has been introduced at time  $t=0.25$  s on the PV array side (rainy time or shadow effect) as it is represented in Fig. 20a. The load voltages and currents represented in Fig. 20b are

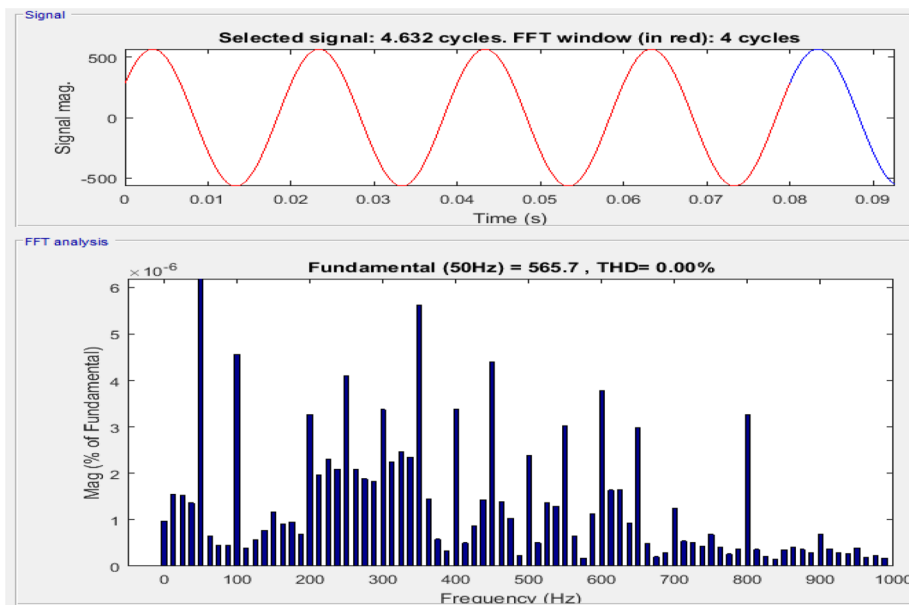


Fig. 17 THD of 0.00% for Vabc with RL-load

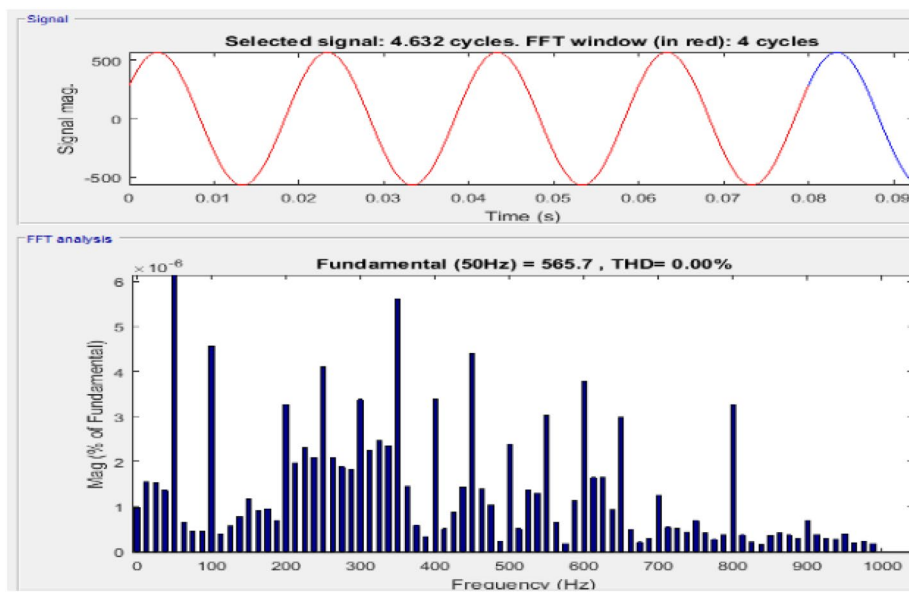
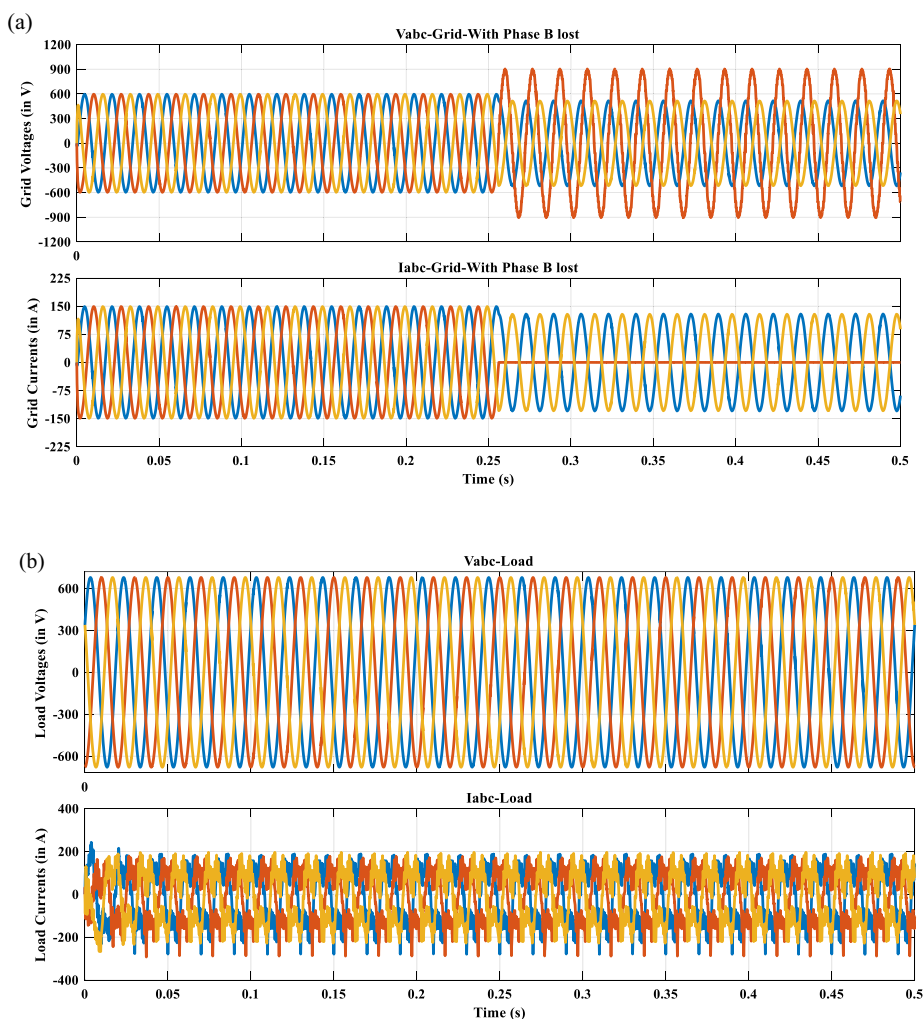


Fig. 18 THD of 0.00% for Vabc with L-load

affected by this failure because the grid continues to supply the load properly. From the obtained results, it can be noted that in case of a fault in one side or another, it does not affect the operation of load. In fact, when there is a phase lost failure from the grid, the PV system continues to supply the load properly. Also, in case of shadow or during a raining day, the grid supplies the load properly. The control technique has improved the smooth operation of the whole system, compared to results obtained those obtained in previous researches like in [6, 13, 15, 16].



**Fig. 19** Effect of the grid failure on the operation of the load: **a** grid voltages and currents, **b** load voltages and currents

**Conclusion**

This paper presents the study of a PV system with a developed MPP controller. From the theory of the photovoltaic, a mathematical model of the PV has been presented. The system has been simulated with MATLAB/SIMULINK. A five-level VSI interconnected to grid controlled by SRF structure with PD multicarrier modulation technique is analysed. The connection to grid by means of inverter is synchronized, and the power from the PVA is injected to the system compensating the loads connected. First, the simulations of the PVA showed that the simulated models were accurate to determine the characteristic voltage and current because the current and voltage characteristics are the same as the characteristic given from the data sheet. When the irradiance changes, the PVA output voltage and current also change. The simulation showed that INC algorithm can track the MPP of the PV; thus, the system runs at maximum power no matter what

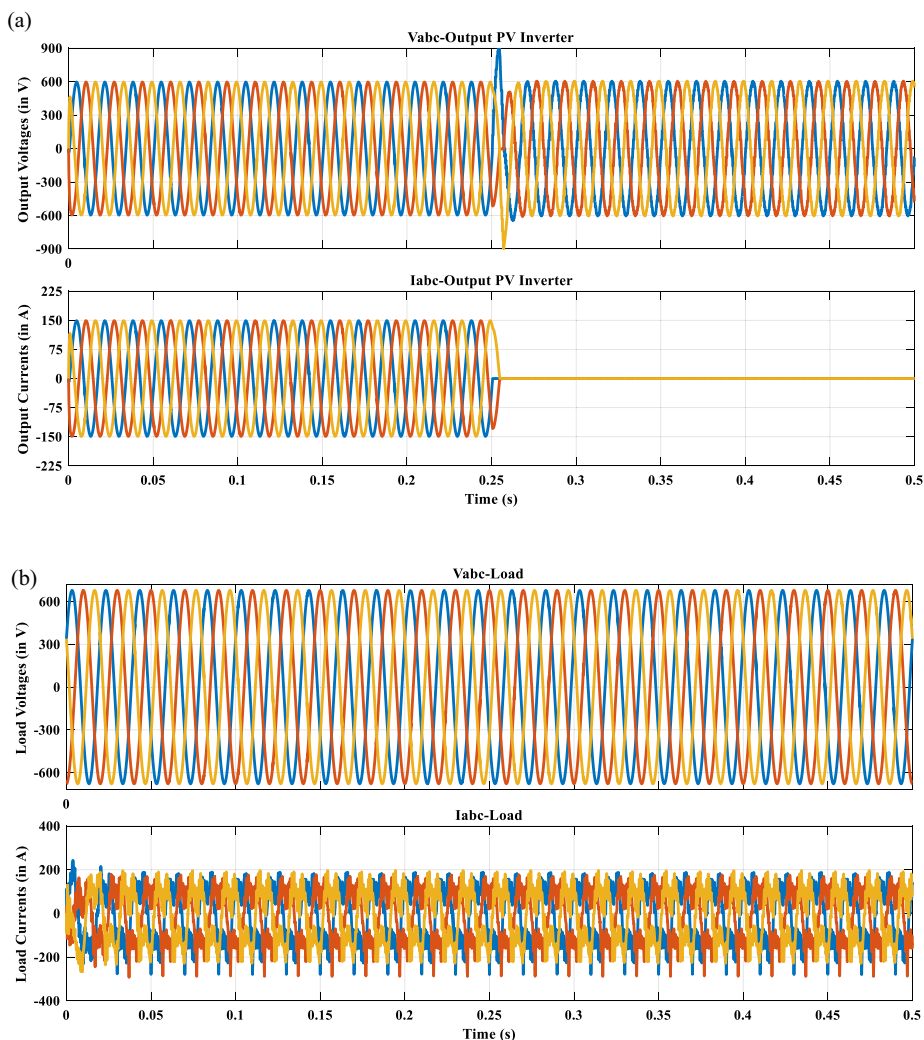


**Fig. 20** Effect of the PV array failure on the operation of the load: **a** grid voltages and currents, **b** load voltages and currents

the operation conditions are. The results showed that INC algorithm delivered efficiency close to 100% in steady state. The simulation of the system was performed with RL-load and L-load and %THD gotten through FFT analysis. The results showed that the load is supplied properly even if there is a failure either on the PVA side or on the grid side. With the robust controlled method used, this grid-tied system is suitable to solve major problems faced by some critical loads, which need to be continuously supplied.

**Acknowledgements**

This research did not receive any specific grant from funding agencies in the public, commercial, or not-for-profit sectors.

**Author contributions**

AB carried all the major works in this study. From data collection to the simulations with MATLAB®/SIMULINK®, AB conceived the study, designed and coordinated the team to produce the draft of the manuscript. PK carried out the proofreading work of the manuscript. He also provided some key features of using MATLAB®/SIMULINK®. All authors read and approved the final manuscript.

**Funding**

This research work did not receive any funding.

**Availability of data and materials**

Data used in this research work are available under request.



## Declarations

### Competing interests

No author associated with this paper has declared any potential or pertinent conflicts, which may be perceived to have impending conflict with this work.

Received: 31 January 2023 Accepted: 30 April 2023

Published online: 10 May 2023

## References

1. Hasan K, Othman MM, Meraj ST, Rahman NF, Noor SZ, Musirin I, Abidin IZ (2022) Online harmonic extraction and synchronization algorithm based control for unified power quality conditioner for microgrid systems. In: 2021 8th International conference on power and energy systems engineering (CPESE 2021), vol 8, 10–12 September 2021, Fukuoka, Japan, Energy Reports, pp 962–971
2. Sirisha B, Nazeemuddin MA (2022) A novel five-level voltage source inverter interconnected to grid with SRF controller for voltage synchronization. *Bull Electr Eng Inform* 11:50–58
3. Jately V, Azzopardi B, Joshi J, Sharma A, Arora S (2021) Experimental analysis of hill-climbing MPPT algorithms under low irradiance levels. *Renew Sustain Energy Rev* 150:111467
4. Saidi AS, Salah CB, Errachdi A, Azeem MF, Bhutto JK, Ijyas VT (2021) A novel approach in stand-alone photovoltaic system using MPPT controllers & NNE. *Ain Shams Eng J* 12:1973–1984
5. Mahammedi A, Kouzou A, Hafaifa A, Talbi B (2019) A new technique for a good efficiency of photovoltaic system under fast changing solar irradiation. *Electroteh Electron Autom* 67(4):12–19
6. Raj A, Praveen RP (2022) Highly efficient DC–DC boost converter implemented with improved MPPT algorithm for utility level photovoltaic applications. *Ain Shams Eng J* 13:101617
7. Fathy A, Atitallah AB, Yousri D, Rezk H, Al-Dhaifallah M (2022) A new implementation of the MPPT based raspberry Pi embedded board for partially shaded photovoltaic system. *Energy Rep* 8:5603–5619
8. Karmouni H, Chouiekh M, Motahhir S, Qjidaa H, Jamil MO, Sayyouri M (2022) A fast and accurate sine-cosine MPPT algorithm under partial shading with implementation using arduino board. *Clean Eng Technol* 9:100535
9. Liu B, Zhang Z, Li G, He D, Chen Y, Zhang Z, Li G, Song S (2021) Integration of power decoupling buffer and grid-tied photovoltaic inverter with single-inductor dual-buck topology and single-loop direct input current ripple control method. *Electr Power Energy Syst* 125:106423
10. Kumar DS, Lau P, Sharma A, Khambadkone A, Srinivasan D (2020) Improvement of transient response in grid-tied photovoltaic systems using virtual inertia. *IET Willey*, p 14
11. Sirisha B, Kumar PS (2019) SVPWM based generalized switching schemes for seven level DCMLI including over modulation operation - FPGA implementation. In: TENCON 2019–2019 IEEE region 10 conference (TENCON), pp 2135–2142
12. Ahmed M, Harbi I, Kennel R, Abdelrahman M (2022) Dual-mode power operation for grid-connected PV systems with adaptive DC-link controller. *Arab J Sci Eng* 47:2893–2907. <https://doi.org/10.1007/s13369-021-05916-w>
13. Fan S, Yu Y, Zhang Y, Yang H (2019) Multi-mode synchronized PWM schemes for three-level NPC inverter. In: 22nd International conference on electrical machines and systems (ICEMS), pp 1–5
14. Kim D, Ramadhan UF, Islam SU, Jung S, Yoon M (2022) Design and implementation of novel fault ride through circuitry and control for grid-connected PV system. *Sustainability* 14:9736. <https://doi.org/10.3390/su14159736>
15. Sirisha B, Kumar PS (2019) A simplified and generalized space vector pulse width modulation method including over modulation zone for seven diode clamped inverter—FPGA implementation. *Int J Power Electron* 10(4):350–366
16. Sirisha B (2021) A grid interconnected nested neutral point clamped inverter with voltage synchronization using synchronous reference frame controller. *Int J Appl Power Eng* 10(4):364–372
17. Admire J (2019) Study of a grid-connected photovoltaic system. MSc Thesis, Badji Mokhtar University, Electrical Engineering, ANNABA - ALGERIA

## Publisher's note

Springer Nature remains neutral with regard to jurisdictional claims in published maps and institutional affiliations.